Challenges to the DGP Model from Horizon-Scale Growth and Geometry

Wenjuan Fang,[1] Sheng Wang,[2] Wayne Hu,[2,3] Zoltán Haiman,[4] Lam Hui,[1] and Morgan May[5]

[1]*Department of Physics, Columbia University, New York, NY 10027*
[2]*Kavli Institute for Cosmological Physics, Enrico Fermi Institute, University of Chicago, Chicago, IL 60637*
[3]*Department of Astronomy and Astrophysics, University of Chicago, Chicago, IL 60637*
[4]*Department of Astronomy, Columbia University, New York, NY 10027*
[5]*Brookhaven National Laboratory, Upton, NY 11973*

(Dated: August 15, 2008)

We conduct a Markov Chain Monte Carlo study of the Dvali-Gabadadze-Porrati (DGP) self-accelerating braneworld scenario given the cosmic microwave background (CMB) anisotropy, supernovae and Hubble constant data by implementing an effective dark energy prescription for modified gravity into a standard Einstein-Boltzmann code. We find no way to alleviate the tension between distance measures and horizon scale growth in this model. Growth alterations due to perturbations propagating into the bulk appear as excess CMB anisotropy at the lowest multipoles. In a flat cosmology, the maximum likelihood DGP model is nominally a 5.3σ poorer fit than ΛCDM. Curvature can reduce the tension between distance measures but only at the expense of exacerbating the problem with growth leading to a 4.8σ result that is dominated by the low multipole CMB temperature spectrum. While changing the initial conditions to reduce large scale power can flatten the temperature spectrum, this also suppresses the large angle polarization spectrum in violation of recent results from WMAP5. The failure of this model highlights the power of combining growth and distance measures in cosmology as a test of gravity on the largest scales.

I. INTRODUCTION

On the self-accelerating branch of the Dvali-Gabadadze-Porrati (DGP) braneworld model [1], cosmic acceleration arises from a modification to gravity at large scales rather than by introducing a form of mysterious dark energy with negative pressure [2]. In this model our universe is a $(3+1)$-dimensional brane embedded in an infinite Minkowski bulk with differing effective strengths of gravity. The relative strengths define a crossover scale on the brane beyond which $(4+1)$-dimensional gravity and bulk phenomena become important.

A number of theoretical and observational problems of the self-accelerating branch of DGP have been recently uncovered. This branch suffers from pathologies related to the appearance of ghost degrees of freedom [3, 4, 5, 6, 7, 8, 9, 10]. Ghosts can lead to runaway excitations when coupled to normal modes and their existence can invalidate the self-accelerating background solution as well as linear perturbations around it.

Observational problems also arise if one posits that ghosts and strong coupling do not invalidate the idea of self-acceleration itself, *i.e.* that our Hubble volume behaves in a manner that is perturbatively close on scales near the horizon to the modified Friedmann equation specified on this branch. These problems fall into two classes, those due to the background expansion history and those due to the growth of structure during the acceleration epoch.

In a flat spatial geometry the DGP model adds only one degree of freedom to fit acceleration, the crossover scale. Like ΛCDM, the extra degree of freedom can be phrased as the matter density relative to the critical density. Remarkably, with this one parameter, the ΛCDM model can fit three disparate sets of distance measures: the local Hubble constant and baryon acoustic oscillations, the relative distances to high-redshift supernovae (SNe), and the acoustic peaks in the cosmic microwave background (CMB). The flat DGP model cannot fit these observations simultaneously and the significance of the discrepancy continues to grow. The addition of spatial curvature can help alleviate some, but not all, of this tension [11, 12, 13].

On intermediate scales that encompass measurements of the large scale structure of the Universe, the early onset of modifications to the expansion also imply a substantial reduction in the linear growth of structure which is itself slightly reduced by the modification to gravity [14, 15]. If extended to the mildly nonlinear regime where strong coupling effects may alter growth, this reduction is in substantial conflict with weak lensing data [16].

On scales approaching the crossover scale, which are probed by the CMB, the unique modification to gravity in the DGP model itself strongly alters the growth rate. Here the propagation of perturbations into the bulk requires a $(4+1)$-dimensional perturbation framework [17]. The approximate iterative solutions introduced in Rfn. [18] have been recently verified to be sufficiently accurate by a more direct calculation [19] but still are computationally too expensive for Monte Carlo explorations of the DGP parameter space. More recently, a $(3+1)$-dimensional effective approach dubbed the parameterized post-Friedmann (PPF) framework [20, 21] has been developed that accurately encapsulates modified gravity effects with a closed effective dark energy system. The PPF approach enables standard cosmological tools such as an Einstein-Boltzmann linear theory solver to be applied to the DGP model.

In this *Paper*, we implement the PPF approach to DGP and conduct a thorough study of the tension be-

tween CMB distance, energy density, and growth measures, along with the SNe and local distance measures, across an extended DGP parameter space. We find that even adding epicycles to the DGP model does not significantly improve the agreement with the data. Curvature, while able to alleviate the problem with distances, exacerbates the problem with growth. Changing the initial power spectrum to remove excess power in the temperature spectrum destroys the agreement with recent polarization measurements from the five-year Wilkinson Microwave Anisotropy Probe (WMAP) [22].

The outline of the paper is as follows. In §II we review the impact of the DGP modifications on distance measures and the growth of structure emphasizing an effective dark energy PPF approach that is detailed in Appendix A and compared with a growth-geometry splitting approach in Appendix B. We present the results of the likelihood analysis in §III and discuss these results in §IV.

II. DGP DISTANCE AND GROWTH PHENOMENOLOGY

In the DGP model, gravity remains a metric theory on the brane in a background that is statistically homogeneous and isotropic. Its modifications therefore are confined to the field equations that relate the metric to the matter. Once the metric is obtained, all the usual implications for the propagation of light from distant sources and the motion of matter remain unchanged. In this section, we review the DGP modifications to the background metric, or expansion history, and the gravitational potentials, or linear metric perturbations. We cast these modifications in the language of an effective dark energy contribution under ordinary gravity [20, 21, 23, 24, 25, 26, 27].

A. Background Evolution

That the DGP model is a metric theory in a statistically homogeneous and isotropic universe imposes a background Friedmann-Robertson-Walker (FRW) metric on the brane. The FRW metric is specified by two quantities, the evolution of the scale factor a and the spatial curvature K. The DGP model modifies the field equation, *i.e.* the Friedmann equation, relating the evolution of the scale factor $H = a^{-1}da/dt$ to the matter-energy content. On the self-accelerating branch it becomes (see, *e.g.*, Rfns. [2, 28])

$$H^2 = \left(\sqrt{\frac{8\pi G}{3}\sum_i \rho_i + \frac{1}{4r_c^2}} + \frac{1}{2r_c}\right)^2 - \frac{K}{a^2}, \quad (1)$$

where r_c is the crossover scale and subscript i labels the true matter-energy components of the universe to be distinguished below from the effective dark energy contribution.

On the other hand, given the metric the matter evolves in the same way as in ordinary gravity

$$\dot\rho_i = -3aH(\rho_i + P_i). \quad (2)$$

Overdots represent derivatives with respect to conformal time $\eta = \int dt/a$. From these relations, one sees that as $a \to \infty$, $H \to r_c^{-1}$ and the Universe enters a de Sitter phase of accelerated expansion.

In the limit that $r_c \to \infty$ the ordinary Friedmann equation is recovered. The effect of a finite r_c compared with the Hubble scale can be encapsulated in a dimensionless parameter Ω_{r_c} much like the usual contributions of the density $\Omega_i = 8\pi G\rho_i/3H_0^2$ and curvature $\Omega_K = -K/H_0^2$ to the expansion rate

$$\Omega_{r_c} \equiv \frac{1}{4r_c^2H_0^2}. \quad (3)$$

The modified Friedmann equation (1) today then becomes the constraint equation

$$1 = \left(\sqrt{\Omega_{r_c}} + \sqrt{\Omega_{r_c} + \sum_i \Omega_i}\right)^2 + \Omega_K. \quad (4)$$

It is convenient and instructive to recast the impact of r_c as an effective dark energy component. With the same background evolution, the effective dark energy will have an energy density of

$$\rho_e \equiv \frac{3}{8\pi G}\left(H^2 + \frac{K}{a^2}\right) - \sum_i \rho_i. \quad (5)$$

Conservation of its energy-momentum tensor is guaranteed by the Bianchi identities and requires its "equation of state" $w_e \equiv P_e/\rho_e$ to be given by Eq. (2)

$$w_e = \frac{\sum_i(\rho_i + P_i)}{3(H^2 + a^{-2}K)/8\pi G + \sum_i \rho_i} - 1. \quad (6)$$

If we define Ω_e in the same way as Ω_i, the usual constraint condition applies $\sum_i \Omega_i + \Omega_e + \Omega_K = 1$. Comparing it to Eq. (4), we obtain the following relationship between Ω_e and Ω_{r_c}

$$\Omega_e = 2\sqrt{\Omega_{r_c}(1 - \Omega_K)}. \quad (7)$$

Given w_e and Ω_e, we can now describe the background evolution of the DGP cosmology by using the ordinary Friedmann equation for H. Likewise the Hubble parameter specifies the comoving radial distance

$$D(z) = \int_0^z \frac{dz'}{H(z')}, \quad (8)$$

and the luminosity distance

$$d_L(z) = \frac{(1+z)}{\sqrt{-\Omega_K}H_0}\sin\left(\sqrt{-\Omega_K}H_0\, D(z)\right), \quad (9)$$

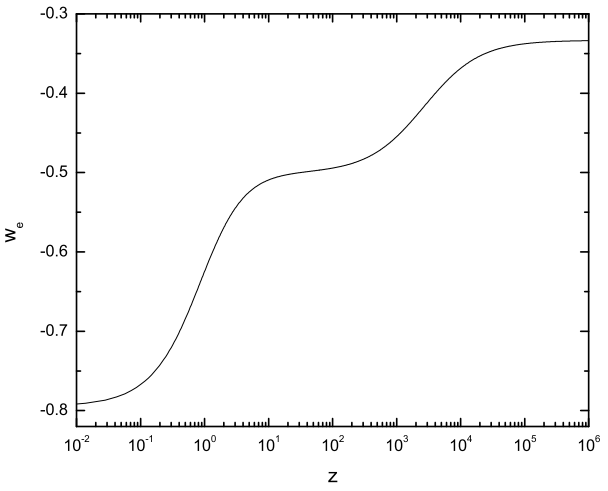

FIG. 1: Equation of state of the effective dark energy w_e for the self-accelerating DGP model with $\Omega_m = 0.26$ and $\Omega_K = 0$.

as usual.

The effective dark energy for DGP has quite a different equation of state from that of a cosmological constant. For example, when there is no curvature, w_e starts at $-1/(1+\Omega_m)$ at the present, approaches $-1/2$ in the matter dominated regime and $-1/3$ in the radiation dominated regime (see Fig. 1).

With the same values of parameters, DGP will have a larger amount of effective dark energy at a given redshift as w_e is always larger than -1, and the universe will expand at a larger rate than in ΛCDM. This reduces the absolute comoving radial distance to a distant source. For relative distance measures like the SNe, the reduction in $H_0 d_L(z)$ can be compensated by lowering the *fractional* contribution of matter through Ω_m. The same is not true for absolute distances, such as those measured by the CMB, baryon oscillations, and Hubble constant, if the overall matter contribution to the expansion rate $\Omega_m H_0^2 a^{-3}$ remains fixed.

B. Structure Formation in the Linear Regime

The same methodology of introducing an effective dark energy component for the background expansion history applies as well to the linear metric perturbations that govern the evolution of large scale structure.

To define the effective dark energy, one must first parameterize the solutions to the $(4+1)$-dimensional equations involving metric perturbations in the brane as well as the bulk [17]. Three simplifications aid in this parameterization [21]. The first is that at high redshift the effect of r_c and the extra dimension goes away rapidly [see Eq. (1)]. The parameterization needs only to be accurate between the matter dominated regime and the present.

Likewise, the predictions of ΛCDM for the relationships between the matter and baryon density at recombination and morphology of the CMB acoustic peaks remain unchanged. As a consequence, the shape of the CMB acoustic peaks still constrains the physical cold dark matter and baryon density $\Omega_c h^2$ and $\Omega_b h^2$ as usual. With these as fundamental high redshift parameters, in a flat spatial geometry, the DGP degree of freedom r_c is then specified by either $\Omega_m = 1 - \Omega_e = \Omega_c + \Omega_b$ or H_0. We shall see below that in a flat universe the competing requirements of CMB and SNe distance measures on r_c will slightly shift the values of $\Omega_c h^2$ and $\Omega_b h^2$ to reach a compromise at the expense of the goodness of fit.

The second simplification is that well below the horizon, perturbations on the brane are in the quasi-static regime where time derivatives can be neglected in comparison with spatial gradients and propagation effects into the bulk are negligible. This allows the equations to be simply closed on the brane by a modified Poisson equation (12) that can be recast as arising from the anisotropic stress of the effective dark energy [14, 15].

The final simplification is that on scales above the horizon, the impact of the bulk perturbations on the brane becomes scale free and depends only on time [18] through dimensionless combinations of H, r_c and K. Furthermore on these scales, generic modifications to gravity are fully defined by the Friedmann equation and the anisotropic stress of the effective dark energy [29, 30].

As shown in Rfn. [21] and detailed in Appendix A, interpolation between these two limits leads to a simple PPF parameterization of DGP on all linear scales. This parameterization has been verified to be accurate at a level substantially better than required by cosmic variance by a direct computation of bulk perturbations [19]. With such a parameterization, efficient Einstein-Boltzmann codes such as CAMB [31] can be modified to calculate the full range of CMB anisotropy, as is done in this paper.

The result of this calculation is that compared with ΛCDM, the growth of structure in the DGP model during the acceleration epoch is suppressed. In the quasi-static regime, this suppression is mostly due to the higher redshift extent of the acceleration epoch discussed in the previous section (see also Fig. 1) with a small component from the effective anisotropic stress or modification to the Poisson equation [14, 15]. On scales approaching r_c, the effect of the anisotropic stress becomes much more substantial due to the perturbations propagating into the bulk [18] resulting in an even stronger integrated Sachs-Wolfe (ISW) effect in the CMB anisotropy power at the lowest multipoles [13].

III. CONSTRAINTS FROM CURRENT OBSERVATIONS

In this section, we employ Markov Chain Monte Carlo (MCMC) techniques to explore constraints on the DGP

parameter space from current observations, and compare them with the successful ΛCDM model. The data we use are: the Supernovae Legacy Survey (SNLS) [32], the CMB anisotropy data from the five-year WMAP [33] for both temperature and polarization (TT + EE + TE), and the Hubble constant measurement from the Hubble Space Telescope (HST) Key Project [34].

We use the public MCMC package *CosmoMC* [35], with a modified version of CAMB for DGP described in Appendix A, to sample the posterior probability distributions of model parameters. The MCMC technique employs the Metropolis-Hastings algorithm [36, 37] for the sampling, and the Gelman and Rubin R statistic [38] for the convergence test. We conservatively require $R-1<0.01$ for the eight chains we run for each model, and this generally gave us ~ 5000 independent samples.

The SNe magnitude-redshift relation probes the relative luminosity distance between the low and high redshift sample. The luminosity distance itself is completely determined by the background expansion history through Eq. (9). On the other hand the power spectra of the CMB anisotropy probes not only the background expansion, but also the growth of structure. To better separate the two types of information, we also consider a canonical scalar field ("quintessence" or QCDM) model with the same expansion history as DGP. This model is defined by the equation of state parameter w_e and density parameter Ω_e in Eqs. (6) and (7).

With only scalar perturbations in consideration, our basic parameter set is chosen to be $\{\Omega_b h^2, \Omega_c h^2, \theta_s, \tau, n_s, A_s\}$, which in turn stand for the density parameters of baryons and cold dark matter, angular size of the sound horizon at recombination, optical depth from reionization (assumed to be instantaneous), spectra index of the primordial curvature fluctuation and its amplitude at $k_* = 0.002$ Mpc^{-1}, *i.e.*, $\Delta^2_\zeta = A_s(k/k_*)^{n_s-1}$. Also, we follow Rfn. [33], and include A_{SZ}, with flat prior of $0<A_{SZ}<2$, to account for the contributions to the CMB power spectra from Sunyaev-Zeldovich fluctuations. The lensing effect on the CMB is neglected. Note that in all the three models we considered, *i.e.* self-accelerating DGP, ΛCDM and QCDM, we have the same parameter sets and priors except that we restrict the DGP parameter space to $H_0 r_c > 1.08$ so that metric fluctuations remain well behaved [see Eq. (16)]. We apply this prior to the QCDM model as well for a fair comparison. In practice, the excluded models are strongly disfavored by the data and the prior is only necessary for numerical reasons.

A. Flat Models

We start with the minimal parameterization of a flat universe with scale free initial conditions. In this case the three model classes ΛCDM, DGP and QCDM all have only one parameter that describes acceleration. In the chain parameters this is θ_s but can be equivalently defined as the derived parameters H_0 or Ω_m. The constraints on the three model classes are given in Table I for the means and marginalized errors on various parameters. Table II shows the best-fit values of the parameters and the corresponding likelihoods, which serve as a "goodness of fit" criterion.

TABLE I: Mean and marginalized errors for various parameters of the self-accelerating DGP, QCDM with the same expansion history as the DGP and ΛCDM models from SNLS + WMAP5 + HST, *assuming a flat universe*. The first 6 parameters are directly varied when running the Markov Chains, while the others are derived parameters, as are in the following tables.

parameters	DGP	QCDM	ΛCDM
$100\Omega_b h^2$	2.36±0.07	2.32±0.07	2.25±0.06
$\Omega_c h^2$	0.090±0.005	0.090±0.005	0.109±0.005
$100\theta_s$	1.042±0.003	1.041±0.003	1.040±0.003
τ	0.10±0.02	0.10±0.02	0.09±0.02
n_s	1.00±0.02	0.99±0.02	0.96±0.01
$\ln[10^{10}A_s]$	3.02±0.05	3.05±0.04	3.18±0.04
H_0	66 ± 2	65±2	72±2
Ω_m	0.26 ± 0.02	0.26±0.02	0.26±0.02
Ω_{r_c}	0.136 ± 0.009	..	..

TABLE II: Parameters and the likelihood values at the best-fit point of the self-accelerating DGP, QCDM with the same expansion history as the DGP and ΛCDM models fitting to SNLS + WMAP5 + HST, *assuming a flat universe*.

parameters	DGP	QCDM	ΛCDM
$100\Omega_b h^2$	2.37	2.32	2.26
$\Omega_c h^2$	0.0888	0.0907	0.110
$100\theta_s$	1.04	1.04	1.04
τ	0.0954	0.0998	0.0825
n_s	0.998	0.983	0.959
$\ln[10^{10}A_s]$	3.01	3.06	3.18
H_0	66.0	65.1	71.6
Ω_m	0.258	0.269	0.258
Ω_{r_c}	0.138	..	..
$-2\ln L$	2805.8	2797.6	2777.8

First, we compare the constraints on the QCDM model with those on ΛCDM. The differences are expected to reflect those between the background expansion histories of the DGP and ΛCDM models. In spite of the clustering effects on the largest scales of a quintessence dark energy, the difference between QCDM and ΛCDM is completely encoded in the equation of state of their dark energy components given the fixed sound speed of quintessence.

Constraints from the SNe magnitudes come from the dimensionless luminosity distance $H_0 d_L(z)$ [see Eq. (9)], once the unknown absolute magnitude is marginalized. In order to match the predictions for $H_0 d_L(z)$ of a flat ΛCDM model, we would expect that the QCDM model has a smaller Ω_m to compensate the larger w_e its dark

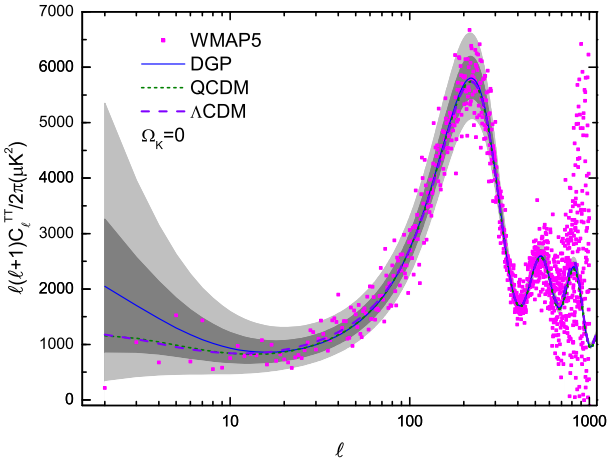

FIG. 2: Predictions for the power spectra of the CMB temperature anisotropies $C_\ell^{\rm TT}$ of the best-fit DGP (solid), QCDM with the same expansion history as DGP (short-dashed), and ΛCDM (dashed, coincident with QCDM at low ℓ) models obtained by fitting to SNLS + WMAP5 (both temperature and polarization) + HST, *assuming a flat universe*. Bands represent the 68% and 95% cosmic variance regions for the DGP model. Points represent WMAP5 measurements; note that noise dominates over cosmic variance for $\ell \gtrsim 500$.

energy has. However, lowering Ω_m also shortens more of the distance to the last scattering surface and hence increases the angular size of the sound horizon (see §II A).

The physical scale of the sound horizon can partially compensate and is controlled by $\Omega_c h^2$ and $\Omega_b h^2$ but these parameters are also well measured by the shape of the peaks and can only be slightly adjusted at a cost to the goodness of fit. Thus the parameter ranges in Table I for $\Omega_c h^2$ decrease and $\Omega_b h^2$ increase slightly which both have the effect of decreasing the angular size of the horizon while Ω_m remains nearly unchanged. This compromise between the energy density and distance constraints results in tension between the CMB and SNe data. This tension shows up as a difference between the $-2\ln L$ values of these two models: $2\ln L(\Lambda\text{CDM}) - 2\ln L(\text{QCDM}) \simeq 20$.

The QCDM model also favors a larger n_s and a smaller A_s. This is a consequence of the larger ISW effect in the QCDM model due to a slower growth rate. Tilting the spectrum can compensate for the excess power in the low-ℓ modes (as shown by the near-coincidence of the short-dashed and dashed curves in Fig. 2).

Next we compare the constraints on the DGP model with those on QCDM. Since the two models have the same expansion history, the differences are entirely caused by the differing growth rates. Due to the propagation of perturbations into the bulk for scales near r_c and the opposite effect of dark energy clustering in QCDM, there is a substantially stronger ISW effect in the first few multipoles of the CMB anisotropy power [13]. Since this effect is only important on the largest angular modes in the CMB TT power spectra which is further limited by the large cosmic variance, the parameter ranges for these two models do not differ significantly. Nonetheless from Fig. 2, it is clear that the best-fit DGP model over predicts the low-ℓ modes anisotropy, though as before, n_s and A_s adjustments try to reduce the primordial perturbations on large scales. This leads to DGP being an even worse fit than QCDM with $2\ln L(\text{QCDM}) - 2\ln L(\text{DGP}) \simeq 8$.

When DGP is compared to ΛCDM, this brings the change in $-2\ln L$ for the maximum likelihood parameters to $\simeq 28$, where $\sim 70\%$ is driven by the background expansion, while $\sim 30\%$ by the dynamical effects on structure growth.

TABLE III: Mean and marginalized errors for various parameters of the self-accelerating DGP, QCDM with the same expansion history as the DGP and ΛCDM models from SNLS + WMAP5 + HST, *allowing curvature*.

parameters	DGP	QCDM	ΛCDM
$100\Omega_b h^2$	2.37±0.07	2.34±0.07	2.25±0.06
$\Omega_c h^2$	0.096±0.006	0.098±0.006	0.108±0.006
$100\theta_s$	1.043±0.003	1.042±0.003	1.040±0.003
τ	0.09±0.02	0.09±0.02	0.09±0.02
Ω_K	0.019±0.008	0.027±0.008	-0.004±0.009
n_s	1.00±0.02	0.99±0.02	0.96±0.01
$\ln[10^{10}A_s]$	3.02±0.05	3.06±0.04	3.18±0.04
H_0	74±4	77±5	70±4
Ω_m	0.22±0.03	0.20±0.03	0.27±0.03
Ω_{r_c}	0.15±0.01	..	..

B. Adding in Curvature

From our analysis in the above section, the flat DGP model is a poor fit to the current observations mostly because it cannot simultaneously satisfy the geometrical requirements of the relative luminosity distances of the SNe and the angular size of the sound horizon at recombination with a single parameter. Since curvature has more of an effect on high redshift distance measures, the tension in the distance measures can be alleviated by including Ω_K in the parameter space [12, 13]. Our results are given in Table III and Table IV.

With curvature, the $-2\ln L$ of the maximum likelihood ΛCDM model almost has no improvement. This is consistent with the results of Rfn. [39], who found strong limits on curvature in ΛCDM, by fitting WMAP5 data combined with SNe or HST. As expected the maximum likelihood model in the QCDM space improves in $-2\ln L$ by ~ 10. The QCDM model needs an open universe to increase the distance to last scattering to compensate the smaller Ω_m, consistent with the findings by

TABLE IV: Parameters and likelihood values at the best-fit point of the self-accelerating DGP, QCDM with the same expansion history as the DGP and ΛCDM models fitting to SNLS + WMAP5 + HST, *allowing curvature*.

parameters	DGP	QCDM	ΛCDM
$100\Omega_b h^2$	2.38	2.36	2.27
$\Omega_c h^2$	0.0937	0.0960	0.107
$100\theta_s$	1.04	1.04	1.04
τ	0.0887	0.0914	0.0884
Ω_K	0.0189	0.0268	-0.00553
n_s	0.996	0.992	0.959
$\ln[10^{10}A_s]$	3.02	3.05	3.18
H_0	73.8	78.3	69.8
Ω_m	0.216	0.195	0.266
Ω_{r_c}	0.149	..	..
$-2\ln L$	2800.8	2787.2	2777.5

[12]. Even with this additional freedom, distance measures remain in slight tension due to the Hubble constant since lowering Ω_m with $\Omega_m h^2$ well determined by the CMB implies a higher Hubble constant [13]. The allowed amount of this shift is limited by the HST Key Project constraint of $H_0 = 72 \pm 8$ km s^{-1} Mpc^{-1}. For QCDM the baryon acoustic oscillation constraint would already disfavor such a shift [40, 41, 42, 43] but its application to DGP requires cosmological simulations of the strong coupling regime. Note that with the distance tension partially removed, the shifts in $\Omega_c h^2$ and $\Omega_b h^2$ are reduced.

The lowering of Ω_m, in addition to the large equation of state parameter of the quintessence, also causes matter domination to terminate at an earlier redshift, and leads to a stronger ISW effect in the QCDM model, as can be seen in Fig. 3, again with a partial compensation from n_s and A_s. The net difference of $-2\ln L$ values of the QCDM model compared to ΛCDM is $\simeq 10$, 50% smaller than before but still a significantly poorer fit.

The situation is even worse for DGP. Here the enhancement of the ISW effect at low Ω_m is even more substantial. Thus the mean value of Ω_K is smaller than the optimal one for the distance constraints in QCDM. Even adjusting the other parameters to give the maximum likelihood model shown in Fig. 3, the poor fit is noticeable at the low multipoles. For example the probability of obtaining a quadrupole as extreme as the observations from the DGP maximum likelihood model is $\sim 1\%$ compared with $\sim 6\%$ for the ΛCDM maximum likelihood model. The net difference in $-2\ln L$ by including curvature as a parameter is only ~ 5 in DGP showing only marginal evidence for curvature in the model at best.

Moreover, the difference from ΛCDM remains substantial with $-2\Delta\ln L \simeq 23$. Since the difference of $-2\Delta\ln L$ from QCDM can be attributed to the ISW effect, $\sim 40\%$ of this difference is driven by the background expansion, and $\sim 60\%$ by the dynamical effects on structure growth.

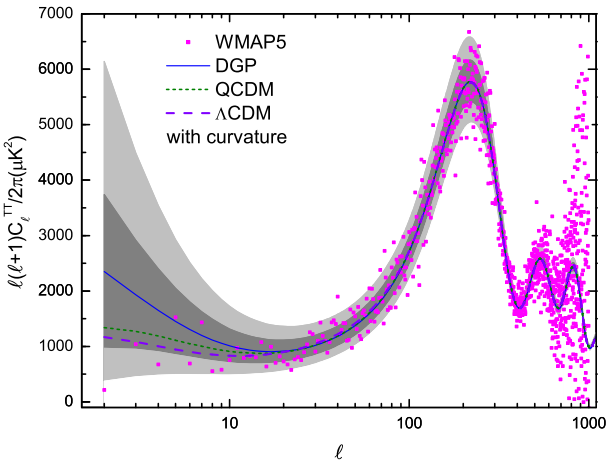

FIG. 3: Predictions for the power spectra of the CMB temperature anisotropies $C_\ell^{\rm TT}$ of the best-fit DGP (solid), QCDM with the same expansion history as DGP (short-dashed), and ΛCDM (dashed) models obtained by fitting to SNLS + WMAP5 (both temperature and polarization) + HST, *allowing curvature*.

C. Changing the Initial Power

The adjustments of A_s and n_s in the above examples suggest that perhaps a more radical change in the initial power spectrum can bring DGP back in agreement with the data. For example, one can sharply reduce large scale power in the temperature spectrum by cutting off the initial power spectrum on large scales, below a wavenumber $k_{\rm min}$. While this is a radical modification and has no particular physical motivation, it is useful to check whether such a loss of power could satisfy the joint temperature and polarization constraints.

CMB polarization at these scales arises from reionization which occurs at a substantially higher redshift than DGP modifications affect. A finite polarization requires not only ionization but also large scale anisotropy at this epoch. Eliminating initial power on these scales eliminates the polarization as well. The EE power in the low multipoles has now been measured at 4-5σ level [22] leading to a significant discrepancy if the large scale power is removed in the model.

Given that including this parameter does not improve the fit, instead of adding it to the MCMC parameter space, we illustrate its effects on the maximum likelihood DGP model in §III B.

By maximizing the likelihood for this model to the TT power alone, we find the best agreement is obtained at $k_{\rm min} = 8\times10^{-4}$ Mpc^{-1}, with $-2\Delta\ln L^{\rm TT} \simeq -12$ compared to $k_{\rm min} = 0$. Model predictions with this $k_{\rm min}$ are plotted in Fig. 4, together with the WMAP 5 year data.

With this power truncation the over prediction prob-

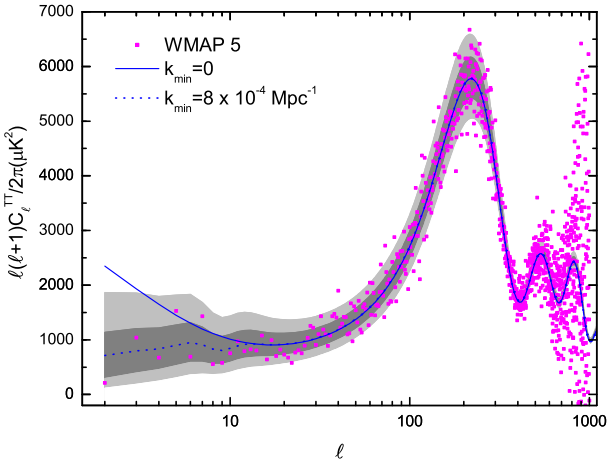

FIG. 4: Predictions for the power spectra of the CMB temperature anisotropies $C_\ell^{\rm TT}$ of the best-fit DGP model as found in §III B without cutting off any large scale primordial perturbations (solid) and with a cut-off scale of $k_{\rm min} = 8 \times 10^{-4}$ Mpc^{-1} (dotted) – the best-fit scale obtained when fitting to the WMAP 5 year TT data alone, while all other parameters are fixed at their best-fit values with $k_{\rm min} = 0$.

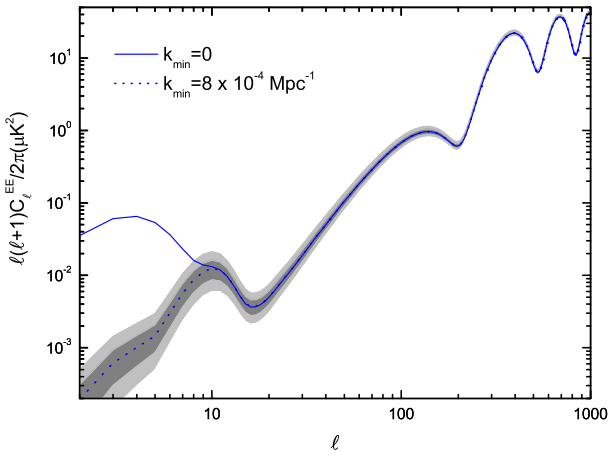

FIG. 5: Predictions for the power spectra of the CMB E-mode polarization $C_\ell^{\rm EE}$ of the best-fit DGP model as found in §III B without cutting off any large scale primordial perturbations (solid) and with a cut-off scale of $k_{\rm min} = 8 \times 10^{-4}$ Mpc^{-1} (dotted) – the best-fit scale obtained when fitting to the WMAP 5 year TT data alone, while all other parameters are fixed their best-fit values. Note here, according to Rfn. [22], the reionization feature at the lowest-ℓ modes is preferred by the data through $\Delta\chi^2 = 19.6$.

lem for the low-ℓ TT power is alleviated, but the EE polarization power on large angular scales is significantly reduced (see Fig. 5). When the polarization data of TE + EE are included, we find $-2\Delta \ln L^{\rm all} \simeq 6$ at $k_{\rm min} = 8 \times 10^{-4}$ Mpc^{-1}, and when $k_{\rm min}$ is varied, the combined data does not favor any positive values of $k_{\rm min}$ as shown in Fig. 6. We conclude that though the DGP model can be made a better fit to the TT power spectrum with a large scale cut-off, polarization measurements are now sufficiently strong to rule out this possibility. While we have only included instantaneous reionization models, changing the ionization history to have an extended high redshift tail can only exacerbate this problem by increasing EE power in the $\ell \sim 10 - 30$ regime [44].

IV. DISCUSSION

We have conducted a thorough Markov Chain Monte Carlo likelihood study of the parameter space available to the DGP self-accelerating braneworld scenario given CMB, SNe and Hubble constant data. To carry out this study, we have introduced techniques for characterizing modified gravity and non-canonical dark energy candidates with the public Einstein-Boltzmann code CAMB that are of interest beyond the DGP calculations themselves.

We find no way to alleviate substantially the tension between distance measures and the growth of horizon scale fluctuations that impact the low multipole CMB temperature and its relationship to the polarization. In

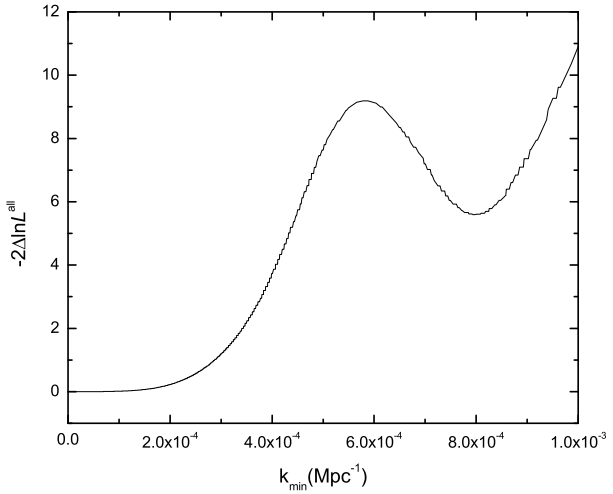

FIG. 6: The total log-likelihood of TT + TE + EE as a function of the cut-off scale $k_{\rm min}$ of the primordial perturbations, shown as the difference from its value at $k_{\rm min} = 0$. We find that when polarization is included, the combined data does not favor any positive values of $k_{\rm min}$. The local minimum shows up at the scale of $k_{\rm min} = 8 \times 10^{-4}$ Mpc^{-1}, which is the one favored by the TT data alone. Note all other parameters are fixed at their best-fit values of the DGP model as found in §III B.

particular we show that the maximum likelihood flat

DGP model is a poorer fit than ΛCDM by $2\Delta \ln L = 28$, nominally a $(2\Delta \ln L)^{1/2} = 5.3\sigma$ result. Interestingly, a substantial ($\sim 30\%$) contribution comes from the change in the growth near the crossover scale where perturbations leak into the bulk.

Adding in spatial curvature to the model can bring the distance measures back in agreement with the data but only at the cost of exacerbating the problem with growth. The net result is that the maximum likelihood only improves by $2\Delta \ln L = 5$ with one extra parameter and the difference from ΛCDM is $2\Delta \ln L = 23$, which is still 4.8σ discrepant with most of the difference arising from the changes to growth.

Furthermore, while the excess power at large angles can be reduced by changing the initial power spectrum to eliminate large scale power, existing WMAP5 CMB polarization measurements already forbid this possibility. Specifically, by introducing any finite cut off to the initial power spectrum to flatten the temperature power spectrum, the global likelihood decreases.

While it is still possible that the resolution of the ghost and strong coupling issues of the theory can alter these consequences, it is difficult to see how they can do so without altering the very mechanism that makes it a candidate for acceleration without dark energy. The failure of this model highlights the power of combining growth and distance measures in cosmology as a test of gravity on the largest scales.

Acknowledgments

We thank K. Koyama and Y.S. Song for useful conversations. This work was supported in part by the NSF grant AST-05-07161, by the Initiatives in Science and Engineering (ISE) program at Columbia University, and by the Polányi Program of the Hungarian National Office for Research and Technology (NKTH). SW and WH were supported by the KICP under NSF PHY-0114422 WH was further supported by U.S. Dept. of Energy contract DE-FG02-90ER-40560 and the David and Lucile Packard Foundation. LH was supported by the DOE grant DE-FG02-92-ER40699, and thanks Alberto Nicolis for useful discussions and Tai Kai Ng at the Hong Kong University of Science and Technology for hospitality. MM was supported by the DOE grant DE-AC02-98CH10886. Computational resources were provided by the KICP-Fermilab computer cluster.

[1] G. R. Dvali, G. Gabadadze and M. Porrati, Phys. Lett. **B 485**, 208 (2000), [arXiv:hep-th/0005016].
[2] C. Deffayet, Phys. Lett. **B 502**, 199 (2001), [arXiv:hep-th/0010186].
[3] M. A. Luty, M. Porrati and R. Rattazzi, JHEP **09**, 029 (2003), [arXiv:hep-th/0303116].
[4] A. Nicolis and R. Rattazzi, JHEP **06**, 059 (2004), [arXiv:hep-th/0404159].
[5] K. Koyama, Phys. Rev. **D 72**, 123511 (2005), [arXiv:hep-th/0503191].
[6] D. Gorbunov, K. Koyama and S. Sibiryakov, Phys. Rev. **D 73**, 044016 (2006), [arXiv:hep-th/0512097].
[7] C. Charmousis, R. Gregory, N. Kaloper and A. Padilla, JHEP **10**, 066 (2006), [arXiv:hep-th/0604086].
[8] C. Deffayet, G. Gabadadze and A. Iglesias, JCAP **0608**, 012 (2006), [arXiv:hep-th/0607099].
[9] G. Dvali, New J. Phys. **8**, 326 (2006), [arXiv:hep-th/0610013].
[10] K. Koyama and F. P. Silva, Phys. Rev. **D 75**, 084040 (2007), [arXiv:hep-th/0702169].
[11] M. Fairbairn and A. Goobar, Phys. Lett. **B 642**, 432 (2006), [arXiv:astro-ph/0511029].
[12] R. Maartens and E. Majerotto, Phys. Rev. **D 74**, 023004 (2006), [arXiv:astro-ph/0603353].
[13] Y.-S. Song, I. Sawicki and W. Hu, Phys. Rev. **D 75**, 064003 (2007), [arXiv:astro-ph/0606286].
[14] A. Lue, R. Scoccimarro and G. D. Starkman, Phys. Rev. **D 69**, 124015 (2004), [arXiv:astro-ph/0401515].
[15] K. Koyama and R. Maartens, JCAP **0601**, 016 (2006), [arXiv:astro-ph/0511634].
[16] S. Wang, L. Hui, M. May and Z. Haiman, Phys. Rev. **D 76**, 063503 (2007), [arXiv:0705.0165].
[17] C. Deffayet, Phys. Rev. **D 66**, 103504 (2002), [arXiv:hep-th/0205084].
[18] I. Sawicki, Y.-S. Song and W. Hu, Phys. Rev. **D 75**, 064002 (2007), [arXiv:astro-ph/0606285].
[19] A. Cardoso, K. Koyama, S. S. Seahra and F. P. Silva, Phys. Rev. **D 77**, 083512 (2008), [arXiv:0711.2563].
[20] W. Hu, Phys. Rev. **D 77**, 103524 (2008), [arXiv:0801.2433].
[21] W. Hu and I. Sawicki, Phys. Rev. **D 76**, 104043 (2007), [arXiv:0708.1190].
[22] WMAP, M. R. Nolta *et al.*, arXiv:0803.0593.
[23] S. Bashinsky, arXiv:0707.0692.
[24] M. Kunz and D. Sapone, Phys. Rev. Lett. **98**, 121301 (2007), [arXiv:astro-ph/0612452].
[25] R. Caldwell, A. Cooray and A. Melchiorri, Phys. Rev. **D 76**, 023507 (2007), [arXiv:astro-ph/0703375].
[26] B. Jain and P. Zhang, arXiv:0709.2375.
[27] E. Bertschinger and P. Zukin, arXiv:0801.2431.
[28] C. Deffayet, S. J. Landau, J. Raux, M. Zaldarriaga and P. Astier, Phys. Rev. **D 66**, 024019 (2002), [arXiv:astro-ph/0201164].
[29] W. Hu and D. J. Eisenstein, Phys. Rev. **D 59**, 083509 (1999), [arXiv:astro-ph/9809368].
[30] E. Bertschinger, Astrophys. J. **648**, 797 (2006), [arXiv:astro-ph/0604485].
[31] A. Lewis, A. Challinor and A. Lasenby, Astrophys. J. **538**, 473 (2000), [arXiv:astro-ph/9911177].
[32] The SNLS, P. Astier *et al.*, Astron. Astrophys. **447**, 31 (2006), [arXiv:astro-ph/0510447].
[33] WMAP, J. Dunkley *et al.*, arXiv:0803.0586, see also http://lambda.gsfc.nasa.gov.
[34] HST, W. L. Freedman *et al.*, Astrophys. J. **553**, 47

(2001), [arXiv:astro-ph/0012376].
[35] A. Lewis and S. Bridle, Phys. Rev. **D 66**, 103511 (2002), [arXiv:astro-ph/0205436], the code and description of its features are available on the Web site: http://cosmologist.info/cosmomc.
[36] N. Metropolis, A. W. Rosenbluth, M. N. Rosenbluth, A. H. Teller and E. Teller, The Journal of Chemical Physics **21**, 1087 (1953).
[37] W. K. Hastings, Biometrika **57**, 97 (1970).
[38] A. Gelman and D. B. Rubin, Statistical Science **7**, 457 (1992).
[39] WMAP, E. Komatsu *et al.*, arXiv:0803.0547.
[40] D. J. Eisenstein *et al.*, Astrophys. J. **633**, 560 (2005), [arXiv:arXiv:astro-ph/0501171].
[41] G. Hütsi, Astron. Astrophys. **459**, 375 (2006), [arXiv:arXiv:astro-ph/0604129].
[42] W. J. Percival *et al.*, Mon. Not. Roy. Astron. Soc. **381**, 1053 (2007), [arXiv:arXiv:0705.3323].
[43] E. Gaztanaga, A. Cabre and L. Hui, ArXiv e-prints (2008), [arXiv:0807.3551].
[44] M. J. Mortonson and W. Hu, arXiv:0804.2631.
[45] T. Giannantonio, Y.-S. Song and K. Koyama, arXiv:0803.2238.
[46] M. Zaldarriaga, U. Seljak and E. Bertschinger, Astrophys. J. **494**, 491 (1998), [arXiv:astro-ph/9704265].
[47] J. Zhang, L. Hui and A. Stebbins, Astrophys. J. **635**, 806 (2005), [arXiv:arXiv:astro-ph/0312348].

APPENDIX A

In Appendix A, we give details of the modification to CAMB employed in the main text to calculate the modified growth of perturbations in the DGP model under the PPF prescription. For perturbations of both the metric and matter in the various gauges, we use the same notations as in Rfn. [20].

1. PPF Description of Modified Gravity in the Linear Regime

Structure formation in the linear regime for a certain class of modified gravity theories can be equivalently described as an effective dark energy component under ordinary gravity. The requirements of this class are that members remain metric theories in a statistically homogeneous and isotropic universe where energy-momentum is conserved. This class includes the self-accelerating branch of the DGP model.

Following Rfns. [20, 21], scalar perturbations for the DGP self-accelerating scenario can be parameterized by three free functions, $g(\eta,k)$, $f_\zeta(\eta)$, and $f_G(\eta)$, and one free parameter c_Γ. We shall see in § 3 that this is equivalent to specifying relationships between the density perturbation, velocity and anisotropic stress of the effective dark energy that close the conservation laws of the effective dark energy.

The metric ratio or anisotropic stress parameter $g(\eta,k)$ is defined as

$$\Phi_+ \equiv g(\eta,k)\Phi_- - \frac{4\pi G}{H^2 k_H^2} P_T \Pi_T \,, \tag{10}$$

where $\Phi_+ \equiv (\Phi+\Psi)/2$, $\Phi_- \equiv (\Phi-\Psi)/2$, with Φ, Ψ as the space-space and time-time metric perturbations in the Newtonian gauge, $k_H = (k/aH)$, Π stands for the anisotropic stress, and the subscript "T" denotes sum over all the true components. When anisotropic stresses of the true components are negligible, g just parameterizes deviations from GR in the metric ratio of Φ_+ to Φ_-.

There are two key features of the PPF parameterization and these define the two additional functions $f_\zeta(\eta)$ and $f_G(\eta)$. The first is that the curvature perturbation in the total matter comoving gauge ζ is conserved up to order k_H^2 in the super-horizon (SH) regime in the absence of non-adiabatic fluctuations and background curvature

$$\lim_{k_H \ll 1} \frac{\dot\zeta}{aH} = -\frac{\Delta P_T - \frac{2}{3} c_K P_T \Pi_T}{\rho_T + P_T} - \frac{K}{k^2} k_H V_T + \frac{1}{3} c_K f_\zeta(\eta) k_H V_T \,, \tag{11}$$

where $f_\zeta(\eta)$ parameterizes the relationship between the metric and the matter. The second is that in the quasi-static (QS) regime, one recovers a modified Poisson equation with a potentially time dependent effective Newton constant

$$\lim_{k_H \gg 1} \Phi_- = \frac{4\pi G}{c_K k_H^2 H^2} \frac{\Delta_T \rho_T + c_K P_T \Pi_T}{1 + f_G(\eta)} \,. \tag{12}$$

Note that even if $f_G = 0$, the Poisson equation for Ψ may also be modified by a non-zero $g(\eta,k)$. In the above two equations, Δ, V and $\Delta P\,(\neq P\Delta)$ are density, velocity, pressure perturbations in the total matter comoving gauge, and $c_K = 1 - 3K/k^2$. To bridge the two regimes, an intermediate quantity Γ is introduced,

$$\Phi_- + \Gamma = \frac{4\pi G}{c_K k_H^2 H^2} (\Delta_T \rho_T + c_K P_T \Pi_T) \,, \tag{13}$$

and an interpolating equation is adopted to make sure it dynamically recovers the behavior specified by Eqs. (11) and (12)

$$(1+c_\Gamma^2 k_H^2)\left[\frac{\dot{\Gamma}}{aH}+\Gamma+c_\Gamma^2 k_H^2(\Gamma-f_G\Phi_-)\right]=S\,. \tag{14}$$

Here the free parameter c_Γ gives the transition scale between the two regimes in terms of the Hubble scale, and the source term S is given by,

$$S=\frac{\dot{g}/(aH)-2g}{g+1}\Phi_-+\frac{4\pi G}{(g+1)k_H^2H^2}\left\{g\left[\frac{(P_T\dot{\Pi}_T)}{aH}+P_T\Pi_T\right]-\left[(g+f_\zeta+gf_\zeta)(\rho_T+P_T)-(\rho_e+P_e)\right]k_HV_T\right\}\,. \tag{15}$$

2. PPF Parameterization for DGP

The PPF parameterization for the self-accelerating DGP is given in Rfn. [21], which we summarize as the follows. On super-horizon scales, the iterative scaling solution developed in Rfn. [18] is well described by

$$g_{\rm SH}(\eta)=\frac{9}{8Hr_c-1}\left(1+\frac{0.51}{Hr_c-1.08}\right)\,, \tag{16}$$

and $f_\zeta(\eta)=0.4g_{\rm SH}(\eta)$, while in the QS regime, the solution is parameterized by [15]

$$g_{\rm QS}(\eta)=-\frac{1}{3}\left[1-2Hr_c\left(1+\frac{\dot{H}}{3aH^2}\right)\right]^{-1}\,, \tag{17}$$

and $f_G(\eta)=0$. On an arbitrary scale in the linear regime, g is then interpolated by

$$g(\eta,k)=\frac{g_{\rm SH}+g_{\rm QS}(c_gk_H)^{n_g}}{1+(c_gk_H)^{n_g}}\,, \tag{18}$$

with $c_g=0.14$ and $n_g=3$. This fitting formula has been shown to give an accurate prediction for the evolution of Φ_- according to the dynamical scaling solution [21]. The transition scale for Γ is set to be $c_\Gamma=1$, *i.e.* at the horizon scale. We note here that the solutions developed in Rfns. [15, 18] are for flat universes, so strictly speaking, the above PPF parameterization only works for DGP with $\Omega_K\to 0$. However for the small curvatures that are allowed by the data, we would expect its effect on structure formation to be small and arise from terms such as $H^2\to H^2+K/a^2$ (see, *e.g.*, Rfn. [45]). Given the cosmic variance of the low-ℓ multipoles, these corrections should have negligible impact on the results.

3. "Dark Energy" Representation of PPF

By comparing the equations that the PPF quantities satisfy with their counterparts in a dark energy system under general relativity, we obtain the following relations for the perturbations of PPF's corresponding effective dark energy. These relations act as the closure conditions for the stress energy conservation equations of the effective dark energy. The first closure condition is a relationship between the PPF Γ variable and the components of the stress energy tensor of the effective dark energy

$$\rho_e\Delta_e+3(\rho_e+P_e)\frac{V_e-V_T}{k_H}+c_KP_e\Pi_e=-\frac{k^2c_K}{4\pi Ga^2}\Gamma\,. \tag{19}$$

The second closure condition is a relationship for the anisotropic stress

$$P_e\Pi_e=-\frac{k_H^2H^2}{4\pi G}g\Phi_-\,. \tag{20}$$

Stress energy conservation then defines the velocity perturbation

$$\frac{V_e-V_T}{k_H}=-\frac{H^2}{4\pi G(\rho_e+P_e)}\frac{g+1}{F}\left[S-\Gamma-\frac{\dot{\Gamma}}{aH}+f_\zeta\frac{4\pi G(\rho_T+P_T)}{H^2}\frac{V_T}{k_H}\right]\,, \tag{21}$$

with

$$F = 1 + \frac{12\pi G a^2}{k^2 c_K}(g+1)(\rho_T + P_T)\,. \tag{22}$$

For details of all the derivations, see Rfn. [20]. The PPF equation for Γ then replaces the continuity and Navier-Stokes equations for the dark energy. Note that the effective dark energy pressure perturbation is not used.

4. Modifying CAMB to Include PPF

Given the dark energy representation of PPF, we only need to modify the parts in CAMB where dark energy perturbations appear explicitly or are needed, in addition to its equation of state which will be specified by the desired background expansion. These include the Einstein equations and the source term for the CMB temperature anisotropy. Since CAMB adopts the synchronous gauge, in this section, we will express everything in the same gauge.

The two Einstein equations used in CAMB are,

$$\frac{\dot{h_L}}{2k} - c_K k_H \eta_T = \frac{4\pi G}{k_H H^2}(\rho_T \delta_T^s + \rho_e \delta_e^s)\,, \tag{23}$$

$$k\dot{\eta_T} - K\frac{(\dot{h_L} + 6\dot{\eta_T})}{2k} = 4\pi G a^2\left[(\rho_T + P_T)v_T^s + (\rho_e + P_e)v_e^s\right]\,, \tag{24}$$

where h_L, η_T are metric perturbations, δ, v are density and velocity perturbations, and superscript "s" labels the synchronous gauge. Here, we only need to provide δ_e^s and v_e^s. Given the gauge transformation relation for velocity

$$V = v^s + k\alpha\,, \tag{25}$$

with $\alpha \equiv (\dot{h_L} + 6\dot{\eta_T})/2k^2$, the following expression for v_e^s is easily obtained from Eq. (21)

$$(\rho_e + P_e)v_e^s = (\rho_e + P_e)v_T^s - \frac{k_H H^2}{4\pi G}\frac{(g+1)}{F}\left[S - \Gamma - \frac{\dot{\Gamma}}{aH} + f_\zeta \frac{4\pi G(\rho_T + P_T)(v_T^s + k\alpha)}{k_H H^2}\right]\,. \tag{26}$$

In order to calculate v_e^s, we need to evaluate α, which we find, with the help of the first closure condition and the two Einstein equations, to be given by

$$k\alpha = k_H \eta_T + \frac{4\pi G}{c_K k_H H^2}\left[\rho_T \delta_T^s + \frac{3(\rho_T + P_T)v_T^s}{k_H}\right] - \frac{4\pi G}{k_H H^2}P_e \Pi_e - k_H \Gamma\,. \tag{27}$$

Here, the anisotropic stress is gauge-independent, and is given by Eq. (20), where Φ_- is given by gauge-transforming the density perturbation in Eq. (13) according to

$$\rho\Delta = \rho\delta^s - \dot{\rho}\frac{v_T^s}{k}\,. \tag{28}$$

In addition to α, we need also to specify S and $\dot{\Gamma}$ in order to get v_e^s. Given Φ_-, S can be calculated by gauge-transforming V_T in Eq. (15), and $\dot{\Gamma}$ then follows from Eq. (14). Provided v_e^s and $P_e\Pi_e$, δ_e^s can be obtained by gauge-transforming the first closure condition

$$\rho_e \delta_e^s = -c_K P_e \Pi_e - 3(\rho_e + P_e)\frac{v_e^s}{k_H} - \frac{c_K k_H^2 H^2}{4\pi G}\Gamma\,. \tag{29}$$

The source term for the CMB temperature anisotropy is given by [46]

$$S_T(\eta, k) = \mathcal{G}\left(\Delta_{T0} + 2\dot{\alpha} + \frac{\dot{v_b^s}}{k} + \frac{\Sigma}{4\bar{b}} + \frac{3\ddot{\Sigma}}{4k^2\bar{b}}\right) + e^{-\kappa}(\dot{\eta_T} + \ddot{\alpha}) + \dot{\mathcal{G}}\left(\frac{v_b^s}{k} + \alpha + \frac{3\dot{\Sigma}}{2k^2\bar{b}}\right) + \frac{3\ddot{\mathcal{G}}\Sigma}{4k^2\bar{b}}\,, \tag{30}$$

where the visibility function $\mathcal{G} \equiv -\dot{\kappa}\exp(-\kappa)$, with $\kappa(\eta)$ the optical depth from today to η for Thomson scattering, $\Delta_{T\ell}$ is the multipole of the temperature anisotropy, v_b^s is the baryon velocity, $\Sigma \equiv \Delta_{T2} - 12_2\Delta_{P2}$, with ${}_2\Delta_{P2}$ the

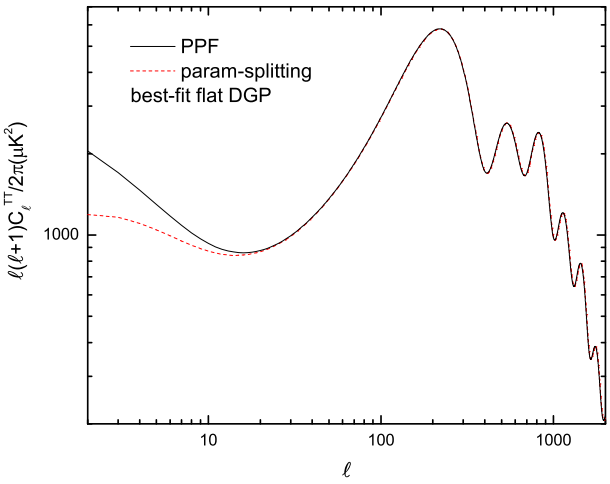

FIG. 7: A comparison of the PPF prediction (upper solid line) with the prediction by parameter-splitting (lower dashed line) for the DGP model.

quadrupole of the polarization anisotropy (for more explicit definitions for $\Delta_{T\ell}$ and ${}_2\Delta_{P\ell}$, see Rfn. [46]), and $\bar{b}^2 = c_K$. Here we need to specify $\dot{\alpha}$ and $\ddot{\alpha}$. $\dot{\alpha}$ is given by the Einstein equation

$$\dot{\alpha} + 2\frac{\dot{a}}{a}\alpha - \eta_T = -\frac{8\pi G}{k_H^2 H^2}(P_T\Pi_T + P_e\Pi_e)\,, \tag{31}$$

Differentiating this equation with respect to η also gives us $\ddot{\alpha}$, which will need the derivative of the effective dark energy's anisotropic stress. From energy-momentum conservation and the first closure condition, we obtain

$$(\dot{P_e\Pi_e}) = \frac{\dot{h_L}}{2}\frac{(\rho_e + P_e)}{c_K} - \frac{k_H^2 H^2}{4\pi G}\dot{\Gamma} + \frac{aH}{c_K}\left\{\delta\rho_e^s + (\rho_e + P_e)v_e^s\left[\frac{6}{k_H} + k_H - \frac{3}{k}\left(\frac{\dot{a}}{a} + \frac{\dot{H}}{H}\right)\right]\right\}\,, \tag{32}$$

which completes our modification of CAMB.

APPENDIX B

In Appendix B, we briefly contrast the PPF prediction for the CMB temperature power spectrum with an attempt to approximate the DGP prediction via the parameter-splitting technique [16, 47]. The technique works by splitting the dark energy equation of state w into two separate parameters, with one, $w_{\rm geometry}$, determining geometric distances and the other, $w_{\rm growth}$, determining the growth of structure. We choose $w_{\rm geometry} = -0.7$ and $w_{\rm growth} = -0.57$, which are obtained respectively by fitting to $H(z)$ (for $z = 0$ to 10) and fitting to the quasi-static growth factor (for $z = 0$ to 2) according to the best-fit flat DGP model (Table II). The result is shown in Fig. 7. One can see that parameter-splitting falls short of the PPF prediction on large angular scales. This illustrates the importance of correctly modeling the perturbation growth on horizon scales. The parameter-split of w does not contain enough freedom to describe perturbation growth in both the sub-horizon (quasi-static) and super-horizon regimes.